

Brief Article

## Structural Biology-Inspired Discovery of Novel KRAS-PDE# Inhibitors

Yan Jiang, Chunlin Zhuang, Long Chen, Junjie Lu, Guoqiang Dong,  
Zhenyuan Miao, Wannian Zhang, Jian Li, and Chunquan Sheng

*J. Med. Chem.*, **Just Accepted Manuscript** • DOI: 10.1021/acs.jmedchem.7b01243 • Publication Date (Web): 20 Sep 2017

Downloaded from <http://pubs.acs.org> on September 20, 2017

### Just Accepted

“Just Accepted” manuscripts have been peer-reviewed and accepted for publication. They are posted online prior to technical editing, formatting for publication and author proofing. The American Chemical Society provides “Just Accepted” as a free service to the research community to expedite the dissemination of scientific material as soon as possible after acceptance. “Just Accepted” manuscripts appear in full in PDF format accompanied by an HTML abstract. “Just Accepted” manuscripts have been fully peer reviewed, but should not be considered the official version of record. They are accessible to all readers and citable by the Digital Object Identifier (DOI®). “Just Accepted” is an optional service offered to authors. Therefore, the “Just Accepted” Web site may not include all articles that will be published in the journal. After a manuscript is technically edited and formatted, it will be removed from the “Just Accepted” Web site and published as an ASAP article. Note that technical editing may introduce minor changes to the manuscript text and/or graphics which could affect content, and all legal disclaimers and ethical guidelines that apply to the journal pertain. ACS cannot be held responsible for errors or consequences arising from the use of information contained in these “Just Accepted” manuscripts.

# Structural Biology-Inspired Discovery of Novel KRAS-PDE $\delta$ Inhibitors

Yan Jiang<sup>†§</sup>, Chunlin Zhuang<sup>†§</sup>, Long Chen<sup>†§</sup>, Junjie Lu<sup>†</sup>, Guoqiang Dong<sup>†</sup>, Zhenyuan Miao<sup>†</sup>, Wannian Zhang<sup>†</sup>, Jian Li<sup>‡</sup>, Chunquan Sheng<sup>†\*</sup>

<sup>†</sup> School of Pharmacy, Second Military Medical University, Shanghai 200433, China

<sup>‡</sup> School of Pharmacy, East China University of Science & Technology, Shanghai 200237, China

Supporting Information

**ABSTRACT:** Structural biology is a powerful tool for investigating the stereospecific interactions between a protein and its ligand. Herein, an unprecedented chiral binding pattern was observed for inhibitors of KRAS-PDE $\delta$  interactions. Virtual screening and X-ray crystallography studies revealed that two enantiomers of a racemic inhibitor could bind at different sites. Fragment-based drug design was used to identify highly potent PDE $\delta$  inhibitors that can be used as promising lead compounds for target validation and antitumor drug development.

## INTRODUCTION

Chirality is a fundamental component of drug-receptor interactions.<sup>1</sup> Generally, enantiomers have different binding affinities for specific biological targets. Structural biology is a powerful tool for clarifying the underlying stereoselectivity of the differential recognition between a protein and chiral substrates and inhibitors. Moreover, chiral promiscuity, such as mirror-image packing, has recently been identified in structural biology studies.<sup>2</sup> However, examples of enantiomers that can be accommodated in different binding pockets in the active site of a protein are rare. Herein, we report a racemic compound that inhibits KRAS-PDE $\delta$  interaction by the binding of its two enantiomers to different hot spots of PDE $\delta$ . This novel chiral binding pattern inspired further fragment-based drug design (FBDD) that facilitated the discovery of a series of highly potent PDE $\delta$  inhibitors (**Figure 1**).

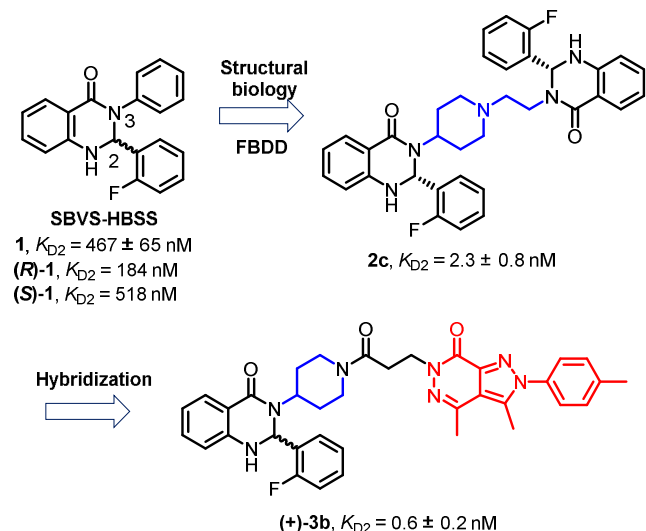


**Figure 1.** Drug design strategies for novel quinazolinone KRAS-PDE $\delta$  inhibitors. Hit **1** was discovered through a structure-based virtual screening, and its preliminary structure-activity relation-

ship (SAR) was clarified by a hit-based substructure search (HBSS). Based on the crystal structure of PDE $\delta$  in complex with compound **1** (PDB entry: 5X72, resolution: 2.50 Å), FBDD was used to link two isomers of compound **1** (PDB entry: 5X73, resolution: 1.95 Å) and generate **2c**, which showed significantly higher activity. Finally, the highly potent PDE $\delta$  inhibitor **(+)-3b** was designed by molecular hybridization.

The KRAS gene is a key regulator in the human body.<sup>3,4</sup> Under normal conditions, the gene is involved in cell growth. Under abnormal conditions, the gene causes sustained cell growth, which leads to cancer. Thus, the product of the gene, KRAS protein, is an important target in anticancer drug discovery.<sup>5,6</sup> The mutation of this protein is common in many cancers, especially in pancreatic (90%), colon (45%) and lung (30%) cancers.<sup>6,7</sup> Mechanistically, mutation of KRAS always occurs via farnesylation at the C-terminal cysteine residue.<sup>3</sup> PDE $\delta$ , also called PDE6D, is the delta subunit of rod specific cyclic GMP phosphodiesterase and plays a critical role in maintaining the dynamic distribution of KRAS in the cell.<sup>8-10</sup> When PDE $\delta$  binds and solubilizes the farnesylated KRAS protein, the diffusion of KRAS is enhanced throughout the cell.<sup>8,11-13</sup> Farnesylated KRAS is then discharged from the PDE $\delta$  prenyl binding pocket by the release factor Arl2 in perinuclear membranes. Next, the KRAS is trapped by the recycling endosome, and its localization to the plasma membrane is restored by vesicular transport. The high concentration of KRAS at the plasma membrane finally results in aberrant oncogenic signaling.<sup>8,14</sup>

At least two strategies have been used for KRAS-based cancer treatment.<sup>5</sup> The first strategy, directly targeting KRAS signaling, has achieved great success but has not been approved as a clinical drug.<sup>15-19</sup> The second strategy, competitive inhibition of KRAS-PDE $\delta$  interaction by small molecules, can be used to reduce the plasma membrane localization of KRAS and its oncogenic signaling.<sup>5,20-23</sup> Recently, several small molecule PDE $\delta$  inhibitors that have shown potential for the treatment of pancreatic cancer have been reported (**S1-S3**, Supporting Information, **Figure S1**).<sup>5,20-22</sup> The benzimidazole inhibitor **S1** (deltarasin) was bound to the prenyl binding pocket of PDE $\delta$  with nanomolar affinity but was non-selective and showed significant toxicity. The pyra-

zolopyridazinone inhibitor **S2** (deltazinone)<sup>21</sup> and the bis-sulfonamide inhibitor **S3** (deltasonamide)<sup>24</sup> showed better selectivity toward PDE $\delta$  than compound **S1**, but their therapeutic effects for pancreatic cancer were far from satisfactory. Thus, novel chemotypes of KRAS-PDE $\delta$  inhibitors are highly desirable for validating the druggability and therapeutic value of the new target.

## RESULTS AND DISCUSSION

**Virtual screening and biochemical activity.** There are two hot spots in the prenyl binding site of PDE $\delta$ , the Arg61 pocket and the Tyr149 pocket, and they are both important for inhibitor binding. Guided by the structural information, structure-based virtual screening (SBVS) of the Specs database was performed to identify novel inhibitors. Using our well established SBVS workflow (Figure S2 in Supporting Information)<sup>25</sup>, 67 molecules were found to bind to both pockets and 54 molecules, representing 39 structural clusters with Tanimoto coefficients <0.8, and were found to have reasonable structures by visual inspection. Ultimately, 40 molecules were subjected to biological evaluation.

Biochemically, the inhibitory ratio disrupting the KRAS-PDE $\delta$  interaction was measured by an established fluorescence anisotropy assay.<sup>5</sup> Initially, all of the compounds were evaluated at a concentration of 5  $\mu$ M, and there were 12 hits with detectable or good KRAS-PDE $\delta$  inhibition (inhibitory ratio > 20%, Table S1 in Supporting Information). Five of the compounds possessed good inhibitory activity with  $K_{D2}$  values ranging from 0.23  $\mu$ M to 3.56  $\mu$ M (Table S1). Two compounds, **1** ( $K_{D2}$  = 467 nM, compound **P9** in Table S1) and **4** ( $K_{D2}$  = 227 nM, compound **P32** in Table S1), showed excellent inhibitory activity in the nanomolar range and reversibly bound to PDE $\delta$  (Supporting Information, Figure S3). Inhibitor **4** showed poor water solubility (0.37  $\mu$ M) and was excluded in further investigations.

Then, an HBSS of the Specs database was performed to select the analogs with dihydroquinazolinone scaffolds that could help clarify the SAR of inhibitor **1**. To explore the effect of C3-phenyl substitutions, a total of 13 compounds were assayed (Supporting Information, Table S2). Generally, the introduction of the substitutions had little impact on the inhibitory activity. Compounds with various halogen and alkyl substitutions showed similar activities ( $K_{D2}$  range: 517 nM ~ 1225 nM). Next, 14 compounds with various C2-substitutions were evaluated (Supporting Information, Table S3). Among them, the initial hit **1**, containing the 2-fluoro substitution, showed the best activity.

**Structural biology and a unique binding mode.** To clarify the accurate binding mode of the new inhibitor **1**, an X-ray crystal structure of PDE $\delta$  complexed with **1** was acquired. Interestingly, when the PDE $\delta$  protein was soaked in racemic **1**, two co-crystals were obtained. First, enantiomers *R*-**1** and *S*-**1** were observed at high resolution (1.95  $\text{\AA}$ ) to bind to the two hot spots of PDE $\delta$  protein (PDB entry: 5X72, Figure 2A), forming a hydrogen bonds with Arg61 and Tyr149, respectively. Second, two molecules of *R*-**1** could also bind to the Arg61 and Tyr149 hotspots (PDB entry: 5X73, resolution: 2.50  $\text{\AA}$ , Figure 2B). In addition to hydrogen bonding interactions with Arg61 and Tyr149, an additional hydrogen bond was formed between the imino group of *R*-**1** and Glu88. To the best of our knowledge, this is the first report of a racemic compound binding to a protein with its enantiomers located in two different pockets. The biochemical results were consistent with the formation of co-crystals. Racemic **1** had a  $K_{D2}$  value of 467 nM and its *R*- and *S*-enantiomers had  $K_{D2}$  values of 184 nM and 518 nM, respectively. The thermal shift assay was carried out to confirm the binding affinity and showed a good correlation with the fluorescence binding assay. As expected, racemic **1** and its *R*- and *S*-enantiomers showed significant increases ( $\Delta T_m$  = 12.7, 14 and 5.75  $^{\circ}\text{C}$ , respectively) in melting temperatures relative to the PDE $\delta$  protein without the inhibitor bound (Supporting Information, Figure S4).

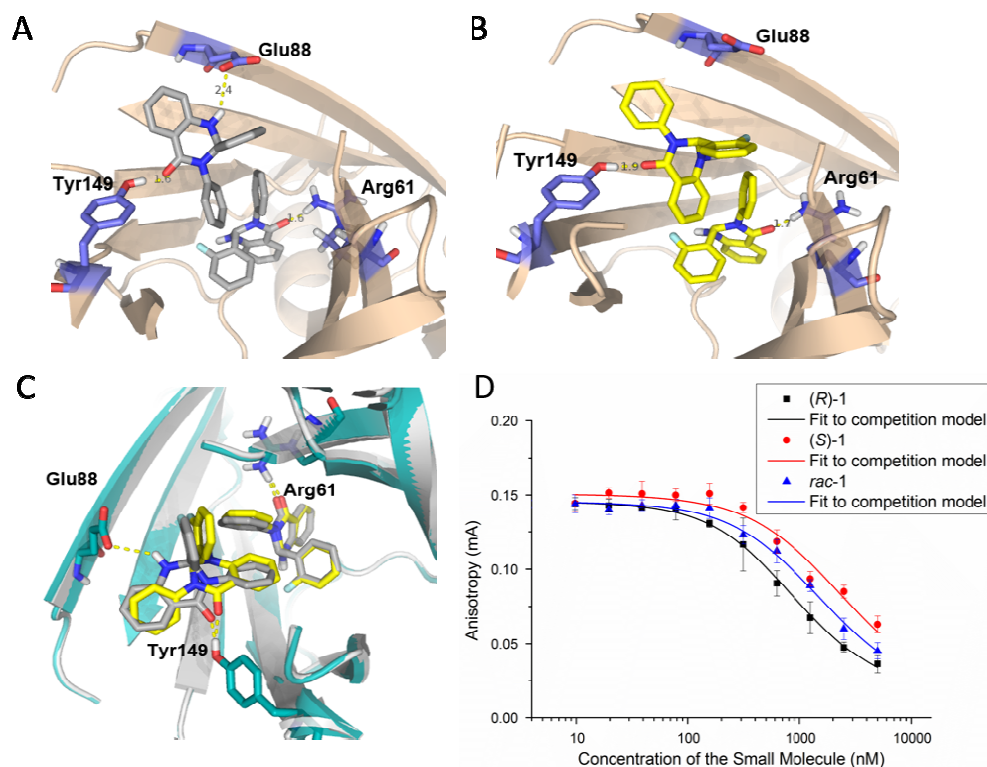
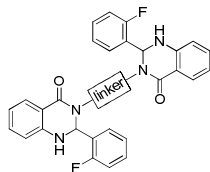


**Figure 2.** Binding mode and inhibitory activity of the novel KRas-PDE $\delta$  inhibitor **1**. (A) Co-crystal complex of two molecules of *R*-**1** with PDE $\delta$  protein (PDB entry: 5X73). (B) Co-crystal complex of one molecule of *R*-**1** and one molecule of *S*-**1** with PDE $\delta$  protein (PDB entry: 5X72). Gln88, Tyr149 and Arg61 are shown as sticks to highlight the hydrogen bonding interactions. Distances for the three hydrogen bonds are shown in yellow. Only the *R*-isomer can be inserted into the Arg61 active pocket, while both isomers can be accommodated in the Tyr149 active pocket. An additional hydrogen bond was observed when the *R*-isomer was in the Tyr149 pocket. (C) Superposition of the two kinds of binding modes. (D) The dose-response curves for the racemic **1** and the two enantiomers using competitive fluorescence anisotropy assay.

**Table 1.** Structures, binding affinities and aqueous solubility of PDE $\delta$  inhibitors designed by FBDD.



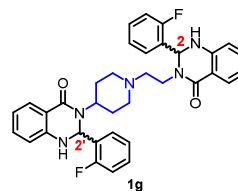
Compound	Linker	Binding affinity <sup>[a]</sup> ( $K_{D2}$ , nM)	Aqueous solubility <sup>[b]</sup> ( $\mu$ M)	cLogP <sup>[d]</sup>
<b>1a</b>		76 $\pm$ 30	N.D. <sup>[c]</sup>	6.38
<b>1b</b>		8 $\pm$ 3	8.9	6.91
<b>1c</b>		4 $\pm$ 2	14	7.44
<b>1d</b>		9 $\pm$ 2	30.9	7.96
<b>1e</b>		15 $\pm$ 3	N.D.	7.96
<b>1f</b>		16 $\pm$ 4	3.2	7.74
<b>1g</b>		12 $\pm$ 5	70.6	5.95
<b>1h</b>		22 $\pm$ 10	N.D.	6.66
<b>S1</b>		24 $\pm$ 9	N.D.	

<sup>[a]</sup> Determined by fluorescence anisotropy assay. <sup>[b]</sup> Determined by HPLC. Compounds were dissolved in water and stirred for 24 h at room temperature. <sup>[c]</sup> Not determined. <sup>[d]</sup> Calculated by ChemDraw 15.1.

**Fragment-based drug design.** The unique binding patterns of inhibitor **1** provided a basis for FBDD. Guided by the conformation of **1** and results of molecular docking, a series of compounds in which two molecules of **1** are connected by various linkers with lengths ranging from 6-12 Å (**1a-1h**, Supporting Information, **Figures S5** and **S6**) were designed and synthesized (Supporting Information, **Scheme S1**). Interestingly, all the compounds showed significantly improved inhibitory activities after being linked to a fragment of **1** (**Table 1**). Compound **1a**, which has a 4-carbon linker, had a  $K_{D2}$  value of 76 nM. Compounds with linkers 5-7 carbons long exhibited higher activities than compounds with shorter linkers. For example, compounds **1b-1d** showed low nanomolar  $K_{D2}$  values. When cyclic linkers such as

cyclohexyl (**1e**), phenyl (**1f**), and piperidiny (**1g-1h**, respectively), were used, the resulting compounds showed potent inhibitory activities. The aqueous solubilities of the five compounds with best inhibitory activities (**1b-1d**, **1f-1g**) were determined to choose a suitable compound for further evaluations (**Table 1**). Among those five compounds, **1g**, with the piperidine linker, had the best combination of activity ( $K_{D2}$  = 12 nM) and solubility (70.6  $\mu$ M, 24 h).

**Table 2.** Biochemical data of the four isomers of compound **1g**.



Compound	Spatial configuration	Binding affinity <sup>[a]</sup> ( $K_{D2}$ , nM)
<b>2a</b>	2 <i>S</i> , 2' <i>S</i> <sup>[b]</sup>	1119 $\pm$ 268
<b>2b</b>	2 <i>S</i> , 2' <i>R</i> <sup>[c]</sup>	33 $\pm$ 12
<b>2c</b>	2 <i>R</i> , 2' <i>R</i> <sup>[d]</sup>	2.3 $\pm$ 0.8
<b>2d</b>	2 <i>R</i> , 2' <i>S</i> <sup>[e]</sup>	57.8 $\pm$ 18

<sup>[a]</sup> Determined by fluorescence anisotropy assay. <sup>[b]</sup> Determined by NMR. <sup>[c]</sup> Determined by single-crystal diffraction. <sup>[d]</sup> Determined by X-ray structural determination. <sup>[e]</sup> Determined by NMR.

Next, chiral separation was performed to isolate the four isomers of compound **1g**. As expected, their activities were significantly different (**Table 2** and **Figure 3D**). The isomers containing the *R*-**1** fragments (**2b-2d**) were more potent than the analogous compounds with the “2*S*, 2'*S*” configurations (**2a**), which is consistent with the biochemical results of compound **1**. The  $K_{D2}$  values of compounds **2b** and **2d**, which both have one *R*-**1** fragment, were similar (33 nM and 57.8 nM, respectively). Compound **2c**, comprised of two tethered *R*-**1** fragments, showed an excellent  $K_{D2}$  value of 2.3 nM, which was comparable to that of compound **S2**. The binding mode of **2c** was further clarified by structural biology studies. The X-ray crystal structure of PDE $\delta$  in complex with inhibitor **2c** revealed that **2c** mimicked the interactions observed for the farnesyl group, meaning it formed hydrogen bonds with Arg61, Glu88 and Tyr149 (**Figure 3A** and **3B**). Superimposition of the two crystal structures of compounds **2c** (PDB entry: 5X74, resolution: 2.24 Å) and *R*-**1** (PDB entry: 5X73, resolution: 2.50 Å) indicated that the original conformations of the two *R*-**1** fragments were mostly retained after fragment linking (**Figure 3C**).

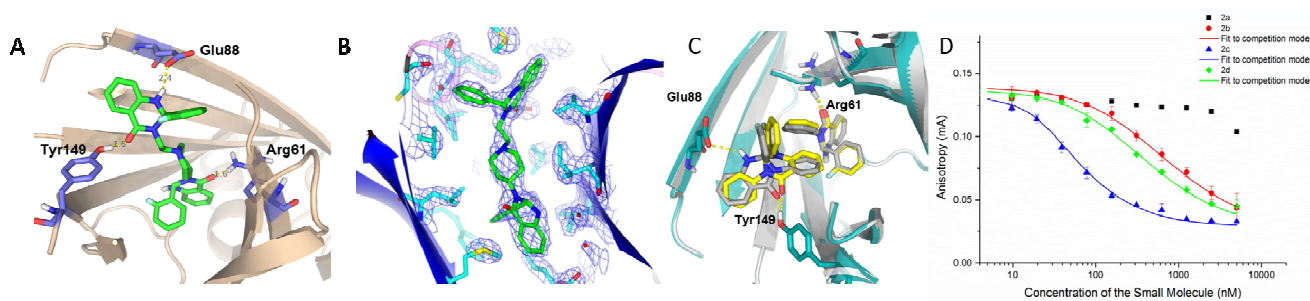


**Figure 3.** The fragment-linking strategy that was used to design the highly potent PDE $\delta$  inhibitor **2c**. (A) Binding mode of **2c** with PDE $\delta$  obtained from a co-crystal complex (PDB entry: 5X74, resolution: 2.24 Å). (B) Electron density maps of the interactions between PDE $\delta$  and **2c**. (C) Superimposition of the X-ray crystal structures of compounds **2c** (PDB entry: 5X74) and **R-1** (PDB entry: 5X73) in the PDE $\delta$  binding pocket. Glu88, Tyr149 and Arg61 are shown as sticks to highlight the hydrogen bonding interactions. Distances for the three hydrogen bonds are shown in yellow. (D) The dose-response curves for the four isomers of compound **1g** using the fluorescence anisotropy assay.

**Table 3.** Biological data of the hybrid molecules.

Compound	Structure	Binding affinity <sup>[a]</sup> ( $K_{D2}$ , nM)	IC <sub>50</sub> ( $\mu$ M) <sup>[b]</sup> Capan-1 cells	Aqueous solubility <sup>[c]</sup> ( $\mu$ M)	cLogP <sup>[e]</sup>
<b>3a</b>		4 $\pm$ 1	27.6 $\pm$ 3.2	403	4.97
<b>3b</b>		2 $\pm$ 0.5	18.6 $\pm$ 1.3	268	3.19
(+)- <b>3b</b>		0.6 $\pm$ 0.2	12.4 $\pm$ 1.7	N.D. <sup>[d]</sup>	
(-)- <b>3b</b>		37 $\pm$ 10	25.6 $\pm$ 4.9	N.D.	
<b>S2</b>		2.2 $\pm$ 0.6	56.9 $\pm$ 5.4	N.D.	3.41

<sup>[a]</sup> Determined by the fluorescence anisotropy assay. <sup>[b]</sup> Determined by the CCK-8 method. <sup>[c]</sup> Determined by HPLC. <sup>[d]</sup> Not determined. <sup>[e]</sup> Calculated by ChemDraw 15.1.

**Cell-based evaluation.** Encouraged by the above results, a cell-based assay was performed. A KRAS-dependent pancreatic cancer cell line (Capan-1) was selected for this evaluation. Unfortunately, compound **1g** showed an inhibition rate of only 48.9% at 100  $\mu$ M. Inspired by the pyrazolopyridazinone scaffold of compound **S2**, that scaffold was used as a replacement for one of the fragments of compound **1** by the molecular hybridization strategy (Table 3 and Scheme S2). Compounds **3a** and **3b** both showed

excellent inhibitory activities. The aqueous solubility of **3a** and **3b** (403 and 268  $\mu$ M, respectively, after 24 h) as well as their anti-tumor activities (IC<sub>50</sub> = 27.6 and 18.6  $\mu$ M, respectively) were significantly better than those of **1g** (70.6  $\mu$ M, 24 h). These results were consistent with the  $K_{D2}$  value of (+)-**3b** being 0.63 nM, which is 58-fold better than that of (-)-**3b**. In Capan-1 cells, (+)-**3b** showed an IC<sub>50</sub> of 12.4  $\mu$ M, which is 4-fold better than that of compound **S2**.

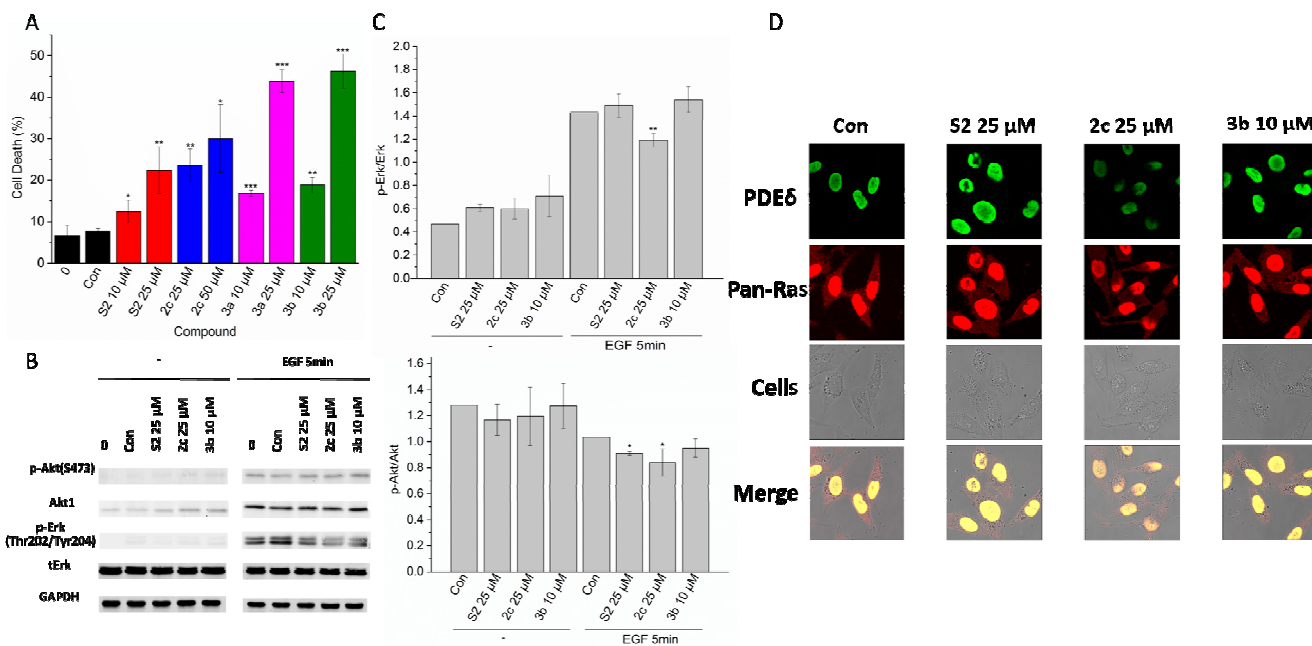


**Figure 4.** Cell-based evaluations of the PDE $\delta$  inhibitors. (A) Apoptosis in the Capan-1 cell line induced by 48 h of treatment with compound **S2**, **2c**, **3a** or **3b**. (B) Cells were treated with compound **S2** (25  $\mu$ M), **2c** (25  $\mu$ M) or **3b** (10  $\mu$ M) for 1 h. Phosphorylation levels were compared between unstimulated and stimulated cells with an epidermal growth factor (EGF) (125 ng/mL, 5 min). From top to bottom: phosphorylated Akt on S473 (pAkt), Akt1, phosphorylated Erk on Thr202 and Tyr204 (pErk), total level of Erk (tErk) and loading control (GAPDH). (C) Gray intensity analysis of the western blots in which quantification of pErk/tErk  $\pm$  SEM (left) and pAkt/Akt  $\pm$  SEM (right) were normalized to the EGF-stimulated control (0.1% DMSO). (D) Immunostaining of Capan-1 with Anti-Pan-RAS (red) and Anti-PDE $\delta$  (green) after treatment with various compounds for 2 h (compound **S2**, 25  $\mu$ M; **2c**, 25  $\mu$ M; **3b**, 10  $\mu$ M). Vehicle control for the above experiments is 0.1% DMSO. \*  $p < 0.05$ , \*\*  $p < 0.01$ .

The cell apoptosis assay indicated that compound **S2** induced a low level of apoptosis (~10%) at 10  $\mu$ M (Figure 4A and Figure S7). Compound **2c** induced apoptosis in 23.6% and 39.3% of the cells at concentrations of 25  $\mu$ M and 50  $\mu$ M, respectively. Compounds **3a** and **3b** also induced apoptosis in a dose-dependent manner (approximately 50% of the apoptotic cells at 25  $\mu$ M), and they were more potent than compound **S2** at the same doses. The RAS family regulates the MAPK and PI3K-Akt-mTOR pathways and subsequently influences cell growth, proliferation and differentiation.<sup>26</sup> Thus, we examined the phosphorylation of extracellular signal-regulated kinase (Erk) and protein kinase B/Akt along these pathways using the oncogenic KRAS-dependent Capan-1 cells with the goal of evaluating the effects of the most potent PDE $\delta$  inhibitors (compounds **2c** and **3b**) on signal transduction. The epidermal growth factor (EGF) could induce MAPK and Akt expression.<sup>27, 28</sup> Phosphorylation levels of Erk and Akt were determined by western blotting before and after 5 min of stimulation with EGF followed by treatment with compound **S2**, **2c** or **3b** for 1 h (Figure 4B and Figure 4C). Compound **S2** (25  $\mu$ M) increased Akt expression as well as EGF but did not induce Erk expression in Capan-1 cells. In contrast, compound **2c** (25  $\mu$ M) downregulated EGF-induced Erk phosphorylation and Akt phosphorylation. EGF-induced Erk and Akt phosphorylation were also downregulated by compound **3b**, but it required a longer incubation time (10  $\mu$ M, > 5 h) (Supporting Information, Figure S8). Immunofluorescence staining of Capan-1 cells showed that compounds **2c** and **3b** induced a distribution of endogenous RAS to endomembranes (Figure 4D). They appeared to downregulate the expression of PDE $\delta$  protein, while compound **S2** was less potent in the induction of RAS distribution. In particular, compound **3b** showed a higher impact on protein expression (10  $\mu$ M) than that of compound **2c** (25  $\mu$ M) and compound **S2** (25  $\mu$ M).

## CONCLUSION

In summary, we have described for the first time that the two isomers of a racemic inhibitor can bind to different pockets of a

target protein. This unique binding pattern was successfully applied to identify highly active PDE $\delta$  inhibitors, whose binding modes were further confirmed by X-ray crystallography. This work provides a novel strategy for chiral drug design targeting protein-protein interactions. Additionally, compounds of this new type of PDE $\delta$  inhibitors can act as valuable chemical probes or lead compounds for investigating the biological functions of KRAS-PDE $\delta$  interactions, validating the druggability of the target and developing novel antitumor agents. Further optimization of the inhibitors is currently ongoing.

## EXPERIMENTAL SECTION

**General.** All reagents and solvents were analytically pure and purchased from the vendors and used without further purification. TLC analysis was carried out on silica gel plates GF254 (Qindao Haiyang Chemical, China). Silica gel chromatography was carried out on 300–400 mesh gel. Anhydrous solvents and reagents were dried by routine protocols. NMR spectra were recorded on a Bruker Avance 600 spectrometers (Bruker Company, Germany), using TMS as an internal standard and CDCl<sub>3</sub> or DMSO-*d*<sub>6</sub> as solvents. Chemical shifts ( $\delta$  values) and coupling constants (*J* values) are given in ppm and Hz, respectively. The mass spectra were recorded on an API-3000 LC-MS mass spectrometer. Purity of the compound was analyzed by HPLC (Agilent 1260) and all final compounds exhibited the purity greater than 95%.

**General procedure A. Synthesis of compounds 1a-1f.** See Scheme S1 in Supporting Information. A solution of 1*H*-benzo[*d*][1,3]oxazine-2,4-dione (2.0 eq), the diamine (1.0 eq) in AcOH was treated with 2-fluorobenzaldehyde (3.0 eq) and refluxed for 4 h. Then, the solution was poured into water (100 mL) and extracted with EtOAc (50 mL $\times$ 3). The combined organic phases were dried and concentrated under reduced pressure. The crude product was purified by column chromatography (hexane/EtOAc = 10:1 ~ 2:1, v/v) to give the target compounds (40%–56% yield).

**General procedure B. Synthesis of compounds 1g-1h.** See Scheme S2 in Supporting Information. A mixture of substituted piperidine (1.0 eq), 3-(2-chloroethyl)-2-(2-fluorophenyl)-2,3-dihydroquinazolin-4(1H)-one (2.0 eq), K<sub>2</sub>CO<sub>3</sub> (4.0 eq), and KI (0.2 eq) in CH<sub>3</sub>CN was refluxed for 24 h. Then, the solvent was removed under the reduced pressure. Water (100 mL) was added and the residue was extracted with EtOAc (50 mL×3). The combined organic phases were dried and concentrated under the reduced pressure. The crude product was purified by column chromatography on silica gel using 1% MeOH in CH<sub>2</sub>Cl<sub>2</sub> as the eluent to afford the target compounds.

**2-(2-Fluorophenyl)-3-(1-(2-(2-(2-fluorophenyl)-4-oxo-1,2-dihydroquinazolin-3(4H)-yl)ethyl)piperidin-4-yl)-2,3-dihydroquinazolin-4(1H)-one (1g).** 30% yield, pale solid. <sup>1</sup>H-NMR (600 MHz, DMSO-*d*<sub>6</sub>) δ 7.65-7.69 (m, 2H), 7.04-7.37 (m, 12H), 6.36-6.68 (m, 4H), 6.20-6.25 (m, 1H), 6.04-6.06 (m, 1H), 4.29-4.32 (m, 1H), 3.74 (s, 1H), 3.02-3.11 (m, 1H), 2.56-2.90 (m, 2H), 2.43 (s, 1H), 2.33 (s, 1H), 1.90-1.96 (m, 1H), 1.49-1.82 (m, 3H), 1.06-1.27 (m, 2H). <sup>13</sup>C NMR (150 MHz, DMSO-*d*<sub>6</sub>) δ 164.31, 163.87, 162.10, 161.31, 160.47, 159.68, 147.76, 146.96, 135.11, 135.05, 132.15, 129.40, 129.25, 129.11, 126.18, 126.02, 119.44, 119.12, 117.78, 117.64, 116.54, 116.25, 67.14, 62.31, 57.43, 54.62, 54.42, 53.10, 43.77, 31.19. HRMS (ESI<sup>+</sup>): m/z calc. for [M+H]<sup>+</sup> C<sub>35</sub>H<sub>34</sub>F<sub>2</sub>N<sub>5</sub>O<sub>2</sub>: 594.2675, found: 594.2682. Purity of the compound was analyzed by HPLC (Agilent 1260) using a Hypersil ODS2 column (eliteHPLC, 4.6\*250 mm, 5 μm) with MeOH: H<sub>2</sub>O = 40:60 as the mobile phase with a flow rate of 0.6 mL/min. HPLC purity: 98.94%, t<sub>R</sub> = 13.46 min.

**3-(1-(3-(3,4-Dimethyl-7-oxo-2-(*p*-tolyl)-2H-pyrazolo[3,4-*d*]pyridazin-6(7H)-yl)propanoyl)piperidin-4-yl)-2-(2-fluorophenyl)-2,3-dihydroquinazolin-4(1H)-one (3b).** Intermediate **m9** (0.1 g, 0.31 mmol, structure see Supporting Information), HATU (0.14 g, 0.37 mmol), and TEA (0.094 g, 0.93 mmol) were dissolved in DMF (10 mL) and stirred at room temperature for 10 min. Then, compound **m5** (0.1 g, 0.31 mmol, structure see Supporting Information) was added, and the resulting mixture was stirred for 1 h and poured into saturated NaCl solution (200 mL). The white precipitate was then filtered, washed with water and dried to afford compound **3b** (0.17 g, 81% yield) as a pale solid. <sup>1</sup>H NMR (600 MHz, CDCl<sub>3</sub>) δ 7.92 (d, 1H, *J* = 8.14 Hz), 7.28-7.35 (m, 4H), 7.17-7.23 (m, 3H), 7.02-7.06 (m, 1H), 6.93-6.96 (m, 1H), 6.78-6.80 (m, 1H), 6.44-6.49 (m, 1H), 6.07-6.09 (m, 1H), 4.94-4.96 (m, 1H), 4.86-4.93 (s, 1H), 4.60-4.78 (m, 1H), 4.73-4.56 (m, 1H), 3.84-4.00 (m, 1H), 2.98-3.14 (m, 1H), 2.86-2.89 (m, 1H), 2.74-2.85 (m, 1H), 2.48-2.65 (m, 1H), 2.43 (d, 1H, *J* = 4.66 Hz), 1.89-1.91 (m, 1H), 1.77-1.84 (m, 1H), 1.52-1.62 (m, 1H), 1.16-1.23 (m, 1H). <sup>13</sup>C NMR (150 MHz, DMSO-*d*<sub>6</sub>) δ 169.06, 168.96, 163.21, 158.49, 156.26, 144.46, 144.41, 141.91, 141.20, 141.16, 139.84, 136.29, 136.00, 133.59, 133.54, 130.38, 130.33, 129.91, 128.53, 128.30, 128.22, 127.75, 125.77, 124.01, 119.51, 117.84, 116.95, 116.86, 115.96, 115.87, 115.81, 115.73, 114.81, 61.21, 51.23, 50.96, 47.18, 45.08, 45.01, 41.18, 41.14, 32.15, 30.47, 30.35, 29.65, 29.39, 21.23, 19.88, 12.28. HRMS (ESI<sup>+</sup>): calc. for [M+H]<sup>+</sup> C<sub>35</sub>H<sub>34</sub>F<sub>2</sub>N<sub>5</sub>O<sub>2</sub>: 634.2936, found: 634.2941. Purity of the compound was analyzed by HPLC (Agilent 1260) using a Hypersil ODS2 column (eliteHPLC, 4.6\*250 mm, 5 μm) with CH<sub>3</sub>CN: H<sub>2</sub>O (0.1% FA) (60:40 to 90:10 over 20 minutes) as the mobile phase with a flow rate of 0.8 mL/min. HPLC purity: 95.47%, t<sub>R</sub> = 5.72 min.

#### ABBREVIATIONS USED

FBDD, fragment-based drug design; SAR, structure-activity relationship; HBSS, hit-based substructure search; SBVS, structure-based virtual screening; PDEδ, protein originally identified as δ-subunit of phosphodiesterase 6, prenyl binding protein; RAS, rat sarcoma (protein); T<sub>m</sub>, protein melting point; MAPK, mitogen-activated protein kinase; Erk, extracellular regulated protein ki-

nases; PI3K, phosphatidylinositol 3 kinase; Akt, protein kinase B(PKB); mTOR, mammalian target of Rapamycin; EGF, epidermal growth factor.

#### ASSOCIATED CONTENT

##### Supporting Information

The Supporting Information is available free of charge on the ACS Publications website.

Detailed experimental procedures, <sup>1</sup>H- and <sup>13</sup>C- NMR spectra, HRMS, results of computational studies, biochemical data of **1** analogs, crystal data of compound **2b**, X-ray data of PDEδ in complex with inhibitors, and all experimental procedures as well as Figures S1–S10 and Tables S1–S9. (DOCX)

X-ray crystallographic data for compound **2b**. (CIF)

Coordinates and structure factors for the PDEδ/quinazolinone inhibitor complexes have been deposited with the Protein Data Bank (www.rcsb.org/pdb) under accession codes 5X72, 5X73, 5X74. Authors will release the atomic coordinates and experimental data upon article publication. (PDB)

SMILES Molecular formula strings (CSV).

#### AUTHOR INFORMATION

##### Corresponding Author

\* Phone / Fax: +86 21 81871239. E-mail: shengcq@smmu.edu.cn

##### Author Contributions

§Yan Jiang, Chunlin Zhuang, Long Chen contributed equally to this work.

All authors contributed to the writing of this manuscript. All authors have approved the final version of the manuscript.

##### Notes

The authors declare no competing financial interests.

#### ACKNOWLEDGMENTS

This work was supported by the National Natural Science Foundation of China (Grant 21738002), the Shanghai Municipal Commission of Health and Family Planning (2017YQ052), and the Shanghai “ChenGuang” Project (16CG42).

#### REFERENCES

- (1) Triggler, D. J. Stereoselectivity of drug action. *Drug Discov. Today* **1997**, *2*, 138-147.
- (2) Bisson, C.; Britton, K. L.; Sedelnikova, S. E.; Rodgers, H. F.; Eadsforth, T. C.; Viner, R. C.; Hawkes, T. R.; Baker, P. J.; Rice, D. W. Mirror-Image packing provides a molecular basis for the nanomolar equipotency of enantiomers of an experimental herbicide. *Angew. Chem. Int. Ed. Engl.* **2016**, *55*, 13485-13489.
- (3) Brunsfeld, L.; Kuhlmann, J.; Alexandrov, K.; Wittinghofer, A.; Goody, R. S.; Waldmann, H. Lipidated Ras and Rab peptides and proteins--synthesis, structure, and function. *Angew. Chem. Int. Ed. Engl.* **2006**, *45*, 6622-6646.
- (4) Gelb, M. H.; Brunsfeld, L.; Hrycyna, C. A.; Michaelis, S.; Tamanoi, F.; Van Voorhis, W. C.; Waldmann, H. Therapeutic intervention based on protein prenylation and associated modifications. *Nat. Chem. Biol.* **2006**, *2*, 518-528.
- (5) Zimmermann, G.; Papke, B.; Ismail, S.; Vartak, N.; Chandra, A.; Hoffmann, M.; Hahn, S. A.; Triola, G.; Wittinghofer, A.; Bastiaens, P. I.; Waldmann, H. Small molecule inhibition of the KRAS-PDEδ interaction impairs oncogenic KRAS signalling. *Nature* **2013**, *497*, 638-642.
- (6) Malumbres, M.; Barbacid, M. RAS oncogenes: the first 30 years. *Nat. Rev. Cancer* **2003**, *3*, 459-465.
- (7) Rocks, O.; Peyker, A.; Kahms, M.; Verveer, P. J.; Koerner, G. C.; Lumbierres, M.; Kuhlmann, J.; Waldmann, H.; Wittinghofer, A.;

- Bastiaens, P. I. An acylation cycle regulates localization and activity of palmitoylated Ras isoforms. *Science* **2005**, *307*, 1746-1752.
- (8) Chandra, A.; Grecco, H. E.; Pisupati, V.; Perera, D.; Cassidy, L.; Skoulidis, F.; Ismail, S. A.; Hedberg, C.; Hanzal-Bayer, M.; Venkataraman, A. R.; Wittinghofer, A.; Bastiaens, P. I. The GDI-like solubilizing factor PDE $\delta$  sustains the spatial organization and signalling of Ras family proteins. *Nat. Cell Biol.* **2011**, *14*, 148-158.
- (9) Nancy, V.; Callebaut, I.; El Marjou, A.; de Gunzburg, J. The delta subunit of retinal rod cGMP phosphodiesterase regulates the membrane association of Ras and Rap GTPases. *J. Biol. Chem.* **2002**, *277*, 15076-15084.
- (10) Nikolova, S.; Guenther, A.; Savai, R.; Weissmann, N.; Ghofrani, H. A.; Konigshoff, M.; Eickelberg, O.; Klepetko, W.; Voswinckel, R.; Seeger, W.; Grimminger, F.; Schermuly, R. T.; Pullamsetti, S. S. Phosphodiesterase 6 subunits are expressed and altered in idiopathic pulmonary fibrosis. *Respir. Res.* **2010**, *11*, 146.
- (11) Ismail, S. A.; Chen, Y. X.; Rusinova, A.; Chandra, A.; Bierbaum, M.; Gremer, L.; Triola, G.; Waldmann, H.; Bastiaens, P. I.; Wittinghofer, A. Arl2-GTP and Arl3-GTP regulate a GDI-like transport system for farnesylated cargo. *Nat. Chem. Biol.* **2011**, *7*, 942-949.
- (12) Chen, Y. X.; Koch, S.; Uhlenbrock, K.; Weise, K.; Das, D.; Gremer, L.; Brunsveld, L.; Wittinghofer, A.; Winter, R.; Triola, G.; Waldmann, H. Synthesis of the Rheb and K-Ras4B GTPases. *Angew. Chem. Int. Ed. Engl.* **2010**, *49*, 6090-6095.
- (13) Zhang, H.; Liu, X. H.; Zhang, K.; Chen, C. K.; Frederick, J. M.; Prestwich, G. D.; Baehr, W. Photoreceptor cGMP phosphodiesterase delta subunit (PDE $\delta$ ) functions as a prenyl-binding protein. *J. Biol. Chem.* **2004**, *279*, 407-413.
- (14) Schmick, M.; Vartak, N.; Papke, B.; Kovacevic, M.; Truxius, D. C.; Rossmannek, L.; Bastiaens, P. I. KRas localizes to the plasma membrane by spatial cycles of solubilization, trapping and vesicular transport. *Cell* **2014**, *157*, 459-471.
- (15) Berndt, N.; Hamilton, A. D.; Sebt, S. M. Targeting protein prenylation for cancer therapy. *Nat. Rev. Cancer* **2011**, *11*, 775-791.
- (16) Bourmet, B.; Buscail, C.; Muscari, F.; Cordelier, P.; Buscail, L. Targeting KRAS for diagnosis, prognosis, and treatment of pancreatic cancer: Hopes and realities. *Eur. J. Cancer* **2016**, *54*, 75-83.
- (17) Maurer, T.; Garrenton, L. S.; Oh, A.; Pitts, K.; Anderson, D. J.; Skelton, N. J.; Fauber, B. P.; Pan, B.; Malek, S.; Stokoe, D.; Ludlam, M. J.; Bowman, K. K.; Wu, J.; Giannetti, A. M.; Starovasnik, M. A.; Mellman, I.; Jackson, P. K.; Rudolph, J.; Wang, W.; Fang, G. Small-molecule ligands bind to a distinct pocket in Ras and inhibit SOS-mediated nucleotide exchange activity. *Proc. Natl. Acad. Sci. U. S. A.* **2012**, *109*, 5299-5304.
- (18) Patgiri, A.; Yadav, K. K.; Arora, P. S.; Bar-Sagi, D. An orthosteric inhibitor of the Ras-SOS interaction. *Nat. Chem. Biol.* **2011**, *7*, 585-587.
- (19) Sun, Q.; Burke, J. P.; Phan, J.; Burns, M. C.; Olejniczak, E. T.; Waterson, A. G.; Lee, T.; Rossanese, O. W.; Fesik, S. W. Discovery of small molecules that bind to K-Ras and inhibit SOS-mediated activation. *Angew. Chem. Int. Ed. Engl.* **2012**, *51*, 6140-6143.
- (20) Zimmermann, G.; Schultz-Fademrecht, C.; Kuchler, P.; Murarka, S.; Ismail, S.; Triola, G.; Nussbaumer, P.; Wittinghofer, A.; Waldmann, H. Structure guided design and kinetic analysis of highly potent benzimidazole inhibitors targeting the PDEdelta prenyl binding site. *J. Med. Chem.* **2014**, *57*, 5435-5448.
- (21) Papke, B.; Murarka, S.; Vogel, H. A.; Martin-Gago, P.; Kovacevic, M.; Truxius, D. C.; Fansa, E. K.; Ismail, S.; Zimmermann, G.; Heinelt, K.; Schultz-Fademrecht, C.; Al Saabi, A.; Baumann, M.; Nussbaumer, P.; Wittinghofer, A.; Waldmann, H.; Bastiaens, P. I. Identification of pyrazolopyridazinones as PDE $\delta$  inhibitors. *Nat. Commun.* **2016**, *7*, 11360.
- (22) Murarka, S.; Martin-Gago, P.; Schultz-Fademrecht, C.; Al Saabi, A.; Baumann, M.; Fansa, E. K.; Ismail, S.; Nussbaumer, P.; Wittinghofer, A.; Waldmann, H. Development of pyridazinone chemotypes targeting the PDE $\delta$  prenyl binding site. *Chem.-Eur. J.* **2017**, *23*, 6083-6093.
- (23) Martin-Gago, P.; Fansa, E. K.; Wittinghofer, A.; Waldmann, H. Structure-based development of PDE $\delta$  inhibitors. *Biol. Chem.* **2017**, *398*, 535-545.
- (24) Martin-Gago, P.; Fansa, E. K.; Klein, C. H.; Murarka, S.; Janing, P.; Schurmann, M.; Metz, M.; Ismail, S.; Schultz-Fademrecht, C.; Baumann, M.; Bastiaens, P. I.; Wittinghofer, A.; Waldmann, H. A PDE6delta-KRas inhibitor chemotype with up to seven H-bonds and picomolar affinity that prevents efficient inhibitor release by Arl2. *Angew. Chem. Int. Ed. Engl.* **2017**, *56*, 2423-2428.
- (25) Zhuang, C.; Narayanapillai, S.; Zhang, W.; Sham, Y. Y.; Xing, C. Rapid identification of Keap1-Nrf2 small-molecule inhibitors through

structure-based virtual screening and hit-based substructure search. *J. Med. Chem.* **2014**, *57*, 1121-1126.

(26) Downward, J. Targeting RAS signalling pathways in cancer therapy. *Nat. Rev. Cancer* **2003**, *3*, 11-22.

(27) Tao, Y.; Gu, Y. J.; Cao, Z. H.; Bian, X. J.; Lan, T.; Sang, J. R.; Jiang, L.; Wang, Y.; Qian, H.; Chen, Y. C. Endogenous cGMP-dependent protein kinase reverses EGF-induced MAPK/ERK signal transduction through phosphorylation of VASP at Ser239. *Oncol. Lett.* **2012**, *4*, 1104-1108.

(28) Dai, H.; Song, D.; Xu, J.; Li, B.; Hertz, L.; Peng, L. Ammonia-induced Na,K-ATPase/ouabain-mediated EGF receptor transactivation, MAPK/ERK and PI3K/AKT signaling and ROS formation cause astrocyte swelling. *Neurochem. Int.* **2013**, *63*, 610-625.

## Table of Contents Graphic

